Research article Available online www.ijsrr.org ISSN: 2279–0543

International Journal of Scientific Research and Reviews

Effect of Al^{3+} Substituent on Elastic Properties of Ni-Cu-Zn Ferrites

B. L. Shinde

Department of Chemistry, Waghire College, Saswad Dist: Pune, 412301 (M.S.) India
E-mail: shindebl1981@gmail.com

ABSTRACT:

Al^{3+} substituted Ni-Cu-Zn ferrites synthesized by the wet chemical co-precipitation method. Sintering temperature determined by TGA-DTA. XRD patterns illustrate sintered ferrites in single phase with cubic spinel structure. The IR spectra recorded in the range 200-800 cm^{-1} indicates two major absorption bands. High frequency bands 'ν_1' is assigned to the tetrahedral and low frequency bands 'ν_2' is assigned to the octahedral complex. SEM image illustrates the prepared samples are amorphous. Elastic moduli and Debye temperature were calculated using IR data and XRD data of prepared ferrite samples. The values of Young's modulus (E), bulk modulus (K) and modulus of rigidity (G) decreased while Debye temperature and stiffness constant increased with Al^{3+}substitution.

KEYWORDS: Ni-Cu-Zn Ferrite, XRD, TGA-DTA, Elastic moduli.

***Corresponding author:**

B. L. Shinde

Department of Chemistry,

Waghire College, Saswad

Dist: Pune, 412301 (M.S.) India

E-mail: shindebl1981@gmail.com

INTRODUCTION

Ferrites are complex magnetic oxides with the ferric oxide (Fe_2O_3) as their basic magnetic component. The spinel ferrites have the general formula MFe_2O_4 with M as divalent metal ions such as Co, Ni, Mg, Fe, Cd, Zn etc. Ferrites having spinel structure are ferromagnetic and have semiconductor properties of type p or n [1, 2]. The spinels are cubic in structure with 8 formula units and possess two sub-lattices. Polycrystalline ferrites exhibiting low hysteresis loss and high resistivity at room temperature are used in microwave applications and radio electronics.[3] The Ni-Zn ferrites are the mainly adaptable ferrites for their high resistivity and low eddy current losses. The high frequency applications and further miniaturization of magnetic components enable the use of NiZn or NiCuZn ferrites, because both of them have high electrical resistivity and can miniaturize magnetic components without a bobbin.[4, 5] The ferrites prepared by different methods such as wet chemical co-precipitation[6], Sol-gel method [7]. Wet chemical methods require low temperature. The elastic moduli represent the mechanical strength and thermal shock resistance of sample. The mostly Ultrasonic pulse transmission method is used to determine the elastic constant.[8] The elastic properties of ferrites determined by using the IR spectroscopy was reported.[9] This article, focused on by the wet chemical co-precipitation method and detailed study of the elastic properties of Al^{3+} substituted $Ni_{0.2}Cu_{0.2}Zn_{0.65}Fe_{2-x}Al_xO4$ ferrites.

EXPERIMENTAL:

Al^{3+} substituted Ni-Cu-Zn ferrites, with nominal composition of $Ni_{0.2}Cu_{0.2}Zn_{0.6}Fe_{2-x}Al_xO_4$ **(**x=0.0 to 0.1 in steps of 0.02) were synthesized by the wet chemical co-precipitation method. The metal sulphates in desired composition dissolved in deionized water to yield clear solution; the initial pH of solution was 3. The 2M NaOH solution used as precipitant, in oxygen atmosphere at 80 ^{O}C, temperature, brownish precipitate of precursor obtained when pH of solution becomes 12. The precipitate was filtered, washed with deionized water till free from sodium sulphates and then dried. Prepared precursors were sintered at 700 °C for 4 h to obtain the ferrites.

TGA/DTA of precursors was carried on SDT Q600 V20.9 Build 20. The X-ray powder diffraction with Cu-K_α radiation (λ=1.5405 Å) by Phillips X-ray diffract meter (Model 3710) used to study crystal structure. The IR spectra recorded in the range 200 to 800 cm^{-1} using Perkin Elmer infrared spectrophotometer. Morphology and structure of the samples were studied on JEOL-JSM-5600 N Scanning Electron Microscope (SEM).

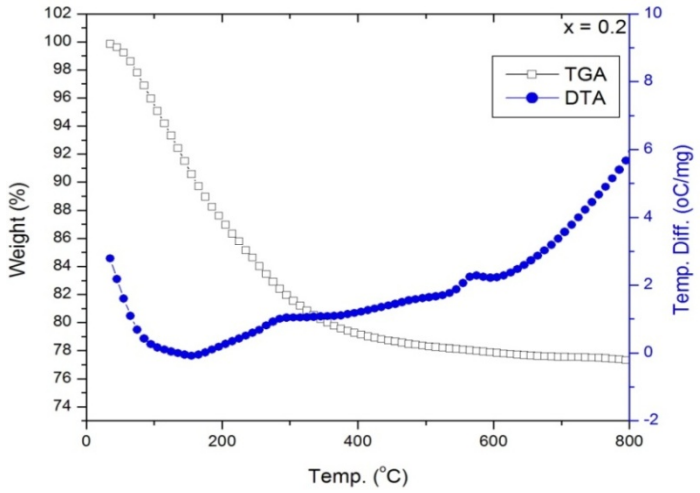

Figure 1: TGA-DTA plot for precursor (x = 0.04)

RESULTS AND DISCUSSION:

The typical TGA/DTA curves of sample (x = 0.04; Fig. 1) shows precursor were dehydrated completely at temperature 175 ^{o}C, and the oxidation takes place in the temperature range 430 ^{o}C and converted in to nano ferrites. No weight loss was observed above 620 °C, therefore, the all the precursors were sintered at 700 °C for 4 hour to obtain the final product.

Figure 2 represents typical XRD pattern for sample x=1.0 illustrate sintered ferrites in single phase with cubic spinel structure without additional peaks corresponding to any other phases. Lattice constant (a), x-ray density and crystallite size of all the samples was determined. The lattice constant, particle size and X-ray density were increases with Al^{3+} concentration.

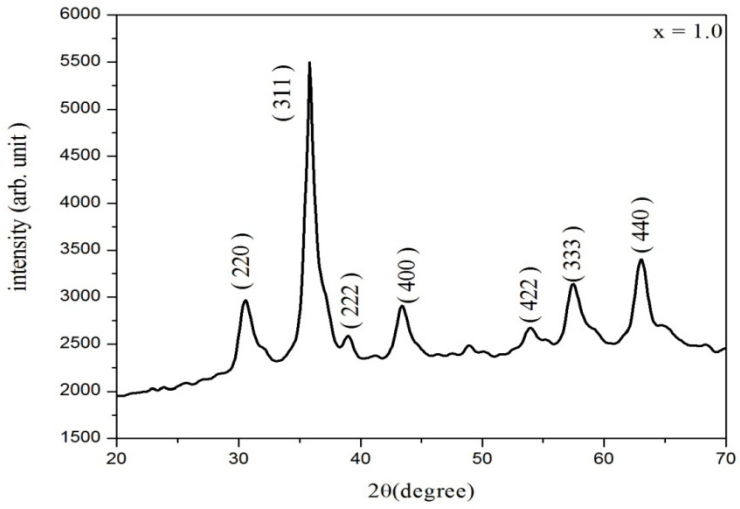

Figure 2. Typical XRD patterns for sample x=1.0

Typical IR spectra recorded in the range 200-800 cm^{-1} of samples (x=0.8) is shown in Fig. 3. High frequency bands (565-593 cm^{-1}) assigned to the tetrahedral and low frequency bands (433-463 cm^{-1}) assigned to the octahedral complex.

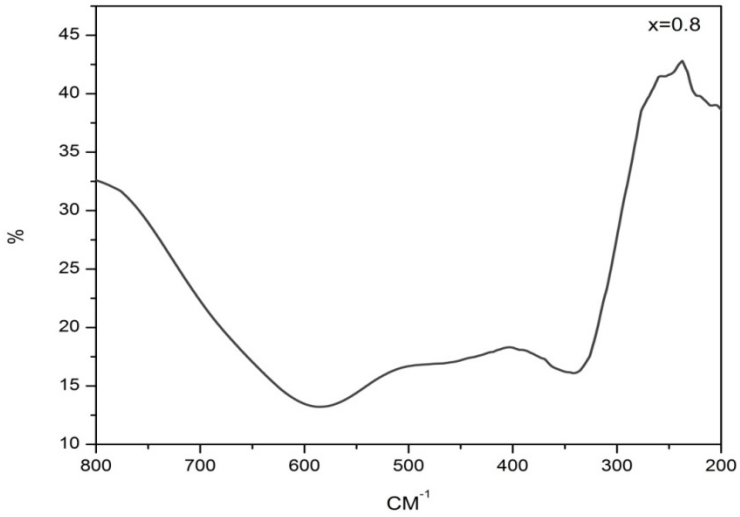

Figure 3: Typical IR spectra x=0.8 for the series

The force constants corresponding to the tetrahedral and octahedral complexes are calculated by using the standard formulae given below[10]:

$$K_t = 7.62 \times M_1 \times \upsilon_1^2 \times 10^{-2} \qquad \text{(i)}$$

$$K_o = 10.62 \times \frac{M_2}{2} \times \upsilon_2^2 \times 10^{-2} \qquad \text{(ii)}$$

Where, K_O is the force constant on octahedral site, K_t is the force constant on tetrahedral site, M_1 molecular weight of tetrahedral site, M_2 molecular weight of octahedral site, ν_1 the corresponding center frequency on tetrahedral site, and ν_2 the corresponding center frequency on octahedral site. It is to be noted that force constant 'K_o' decreased from 2.3818×10^5 to 2.3249×10^5 dyne/cm and K_t decreased from 2.1451×10^5 to 1.9529×10^5 dyne/cm with the substitution of Al^{3+} ions.

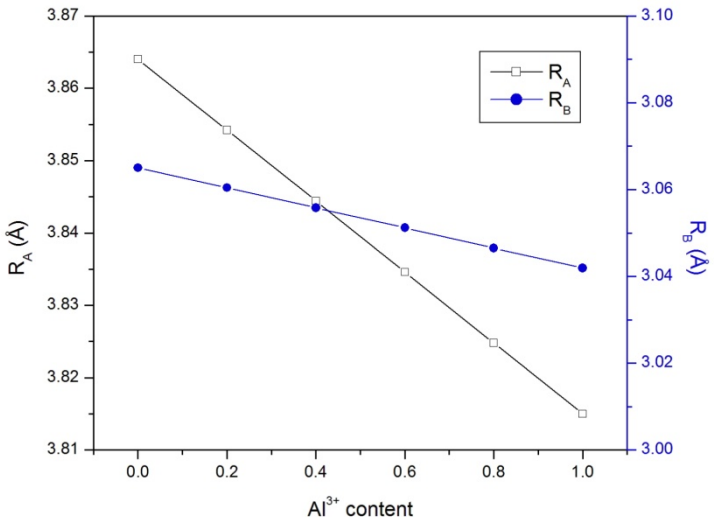

Figure 4: Variation in values of R_A and R_B with Al^{3+} substitution

Table 1 : Mean K, poissons ratio, stiffness constant, elastic moduli and Debye temperature the series.

Comp. x	Mean Force constant $Kx10^2$ (N/m)	Pore Fraction	Poisson's ratio σ	C_{11} (GPa)	C_{12} (GPa)	Youngs modulus	Bulk modulus	Rigdity modulus	Debye Temp. (K)
0.0	1.3385	0.142	0.2760	158.614	60.470	129.404	93.185	50.787	504.34
0.2	1.3661	0.148	0.2740	163.140	61.567	126.802	95.425	50.085	504.368
0.4	1.3127	0.154	0.2720	157.269	58.748	125.316	91.588	49.365	506.589
0.6	1.3013	0.163	0.2689	156.177	57.447	125.28	90.357	49.261	506.831
0.8	1.3083	0.172	0.2659	157.046	56.877	125.232	90.267	49.14	507.487
1.0	1.2639	0.188	0.2605	151.715	53.435	123.879	86.195	49.072	512.483

The average force constant K ($K=K_t+K_o/2$) is given in Table 1. The bond lengths R_A and R_B have been calculated using the formula given by Gorter[11].

$$R_A = \left(u - \frac{1}{4}\right) a_{th}\sqrt{3} - R_o \qquad \text{(iii)}$$

$$R_B = \left(\frac{5}{8} - u\right) a_{th} - R_o \qquad \text{(iv)}$$

The variation in values of R_A, and R_B are given in Fig. 4. Bond lengths R_A and R_B are decreased with the substitution of Al^{3+} ions.

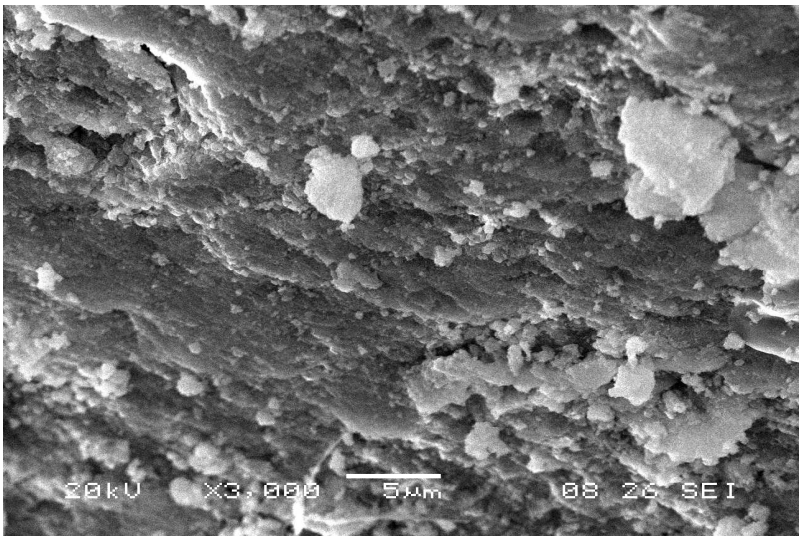

Figure 5: SEM image of sample (x=1.0)

Typical Scanning electron micrograph (SEM) of the sample x=1.0 is shown in Fig. 5. It is observed from the SEM image that the prepared samples are amorphous and porous in nature with agglomeration.

Elastic properties:

Elastic moduli and Debye temperature were determined through IR data and structural data of the series $Ni_{0.2}Cu_{0.2}Zn_{0.6}Fe_{2-x}Al_xO_4$ **(**x=0.0 to 0.1 in steps of 0.02) ferrite samples [9]. The stiffness constant C_{11} was calculated using relation[10],

$$C_{11} = \frac{K}{a} \qquad \text{(v)}$$

Where, K is average force constant and a is lattice constant.

$$(C_{12}) = \frac{\sigma \quad C_{11}}{(1-\sigma)} \qquad \text{(vi)}$$

Where, where σ is Poisson ratio and 'a' is the lattice constant. The Poisson ratio is function of pore fraction. Using equation e and f the stiffness constant is calculated and the variation is tabulated in Table 1. The variation in stiffness constant is illustrated in Fig. 6.

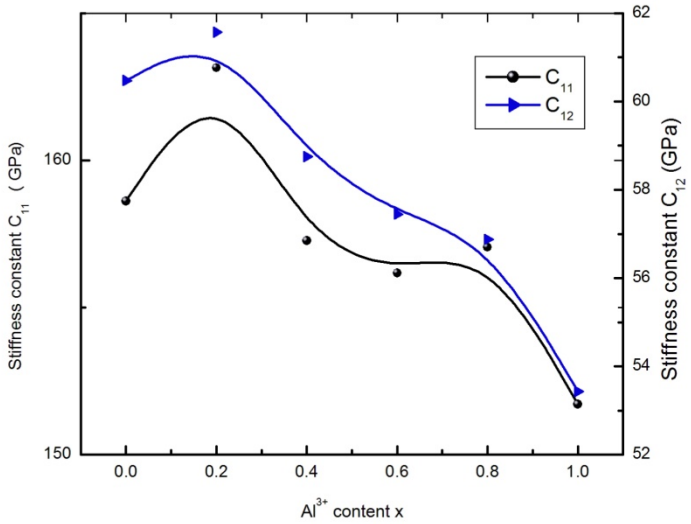

Figure 6: Variation in stiffness constants with Al^{3+} content x

It is observed from Table 1 and Fig. 6 that both the stiffness constants were decreases with increase in Al^{3+} substitution. The values of Poisson's ratio are decreased with the increasing Al^{3+}substitution. The various elastic constants such as; Young's modulus (E), bulk modulus (K) and modulus of rigidity (G) calculated using following equations[12].

$$E = \frac{(C_{11}-C_{12})(C_{11}+2C_{12})}{(C_{11}+C_{12})} \qquad \text{(vii)}$$

$$K = \frac{1}{3}(C_{11} + 2C_{12}) \qquad \text{(viii)}$$

$$G = \frac{E}{2(\sigma+1)} \qquad \text{(ix)}$$

The variation in Young's modulus (E), bulk modulus (K) and modulus of rigidity (G) are presented in Table 1 and Fig. 7. It can be observed from Fig. 7 that the values of Young's modulus (E), bulk modulus (K) and modulus of rigidity (G) modulus decreased with Al^{3+} substitution. The decrease in magnitude of elastic moduli with Al content suggests that the strengthening of interatomic bonding.

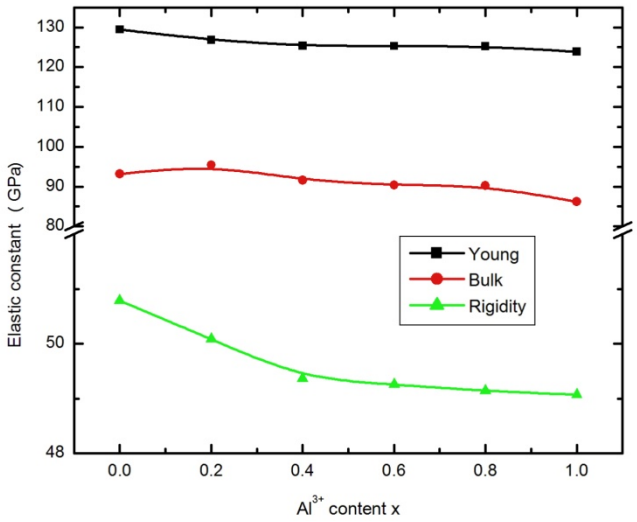

Figure 7: Variation in elastic modulus with Al^{3+} content x

The longitudinal wave velocity (V_L) and Shearing wave velocity (V_S) was calculated using following equations,

$$V_L = \left(\frac{C_{11}}{\rho}\right)^{1/2} \qquad \text{(x)}$$

$$V_S = \left(\frac{G}{\rho}\right)^{1/2} \qquad \text{(xi)}$$

Where, G is rigidity modulus with correct zero pore fraction. The values of V_l and V_s further used to determine mean wave velocity (V_m).[12] The variation in shearing velocity (V_S), mean wave velocity (V_m) and longitudinal wave velocity (V_L), are given in table 1 and Fig. 8.

$$\frac{3}{V_m^{\,3}} = \frac{1}{V_l^{\,3}} + \frac{2}{V_s^{\,3}} \qquad \text{(xii)}$$

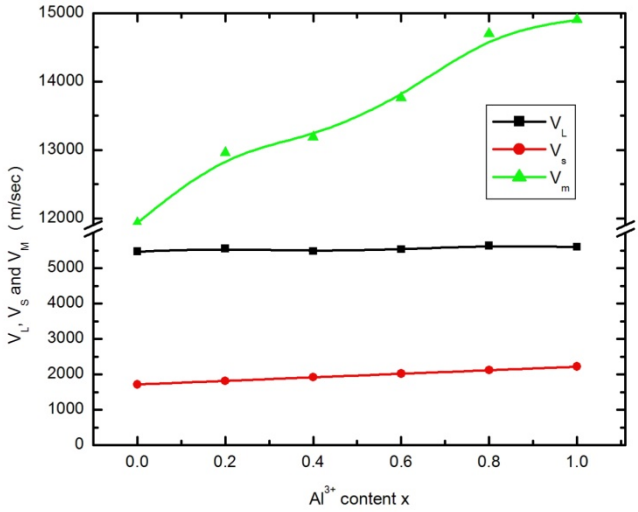

Figure 8: Variation of shearing velocity (V_S), mean wave velocity (V_m) and longitudinal wave velocity (V_L) with Al^{3+} content x

It is observed from Table 1 and Fig. 8, that the shearing velocity (V_S), mean wave velocity (V_m) and longitudinal wave velocity (V_L) increased with Al^{3+} substitution.

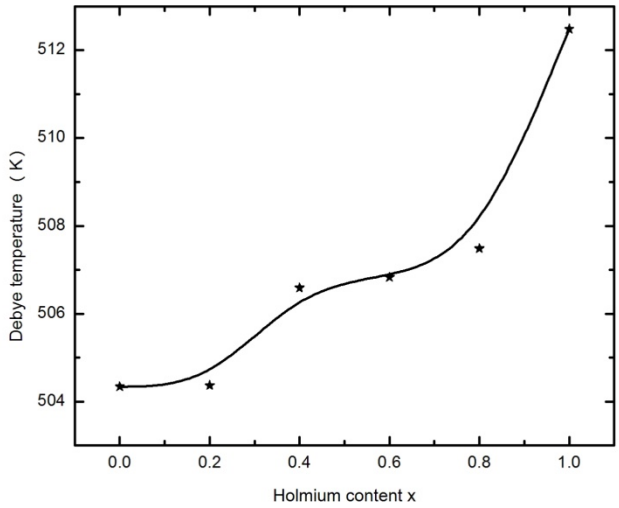

Figure 9: Variation in Debye temperature with Al^{3+} content x

Debye temperature (θ_E) was calculated using following equation[13].

$$\theta_E = \frac{h}{k}\left[\frac{3\rho q N_A}{4\Pi M}\right]^{1/3} \times V_m \qquad \text{(xiii)}$$

Where, h is planks constant, k is Boltzmann's constant, M is molecular weight, q is number if atom in the unit formula and V_m mean wave velocity.

The variation of Debye temperature (θ_E) is given Table 1 and Fig. 9, the Debye temperature increased with Al^{3+} substitution. Debye temperature corresponds to the temperature at which nearly all modes of vibration in solid are excited. Increased values of Debye temperature indicates the increase in the rigidity of the Nickel copper zinc ferrite with increase in Al^{3+} composition x.

4. CONCLUSION:

$Ni_{0.2}Cu_{0.2}Zn_{0.6}Fe_{2-x}Al_xO_4$ **(**x=0.0 to 0.1 in steps of 0.02) synthesized by wet chemical co-precipitation method. High frequency bands (565-593 cm^{-1}) assigned to the tetrahedral and low frequency bands (433-463 cm^{-1}) assigned to the octahedral complex. It is observed from the SEM image that the prepared samples are amorphous and porous in nature with agglomeration. The Poisson's ratio was decreases with increase in Al^{3+} substitution. The values of Young's modulus (E), bulk modulus (K) and modulus of rigidity (G) decreased while Debye temperature and stiffness constant increased with Al^{3+}substitution. Increased values of Debye temperature indicated the increase in the rigidity of the nickel copper zinc ferrite with increase in Al^{3+}composition.

REFERENCES:

1. Fawzi AS, Sheikh AD, Mathe VL. Structural, dielectric properties and AC conductivity of Ni (1− x) ZnxFe2O4 spinel ferrites. Journal of Alloys and Compounds. 2010;502(1):231-7.
2. Naeem M, Shah NA, Gul IH, Maqsood A. Structural, electrical and magnetic characterization of Ni–Mg spinel ferrites. Journal of Alloys and Compounds. 2009; 487(1-2): 739-43.
3. Zaki HM, Al-Heniti SH, Elmosalami TA. Structural, magnetic and dielectric studies of copper substituted nano-crystalline spinel magnesium zinc ferrite. Journal of Alloys and Compounds. 2015; 633:104-14.
4. Matsuo Y, Inagaki M, Tomozawa T, Nakao F. High performance NiZn ferrite. Ieee transactions on magnetics. Jul 2001;37(4):2359-61.
5. Murthy SR. Low temperature sintering of NiCuZn ferrite and its electrical, magnetic and elastic properties. Journal of Materials Science Letters. 2002 Apr 1;21(8):657-60.
6. Darezereshki E. Synthesis of maghemite (γ-Fe2O3) nanoparticles by wet chemical method at room temperature. Materials Letters. 2010 Jul 15;64(13):1471-2.
7. Shinde BL, Dhale LA, Suryavanshi VS, Lohar KS. Preparation and characterization of Chromium-Doped Ni-Cu-Zn Nano Ferrites. Acta Chimica Slovenica. 2017; 64(4):931-7.
8. Raj B, Rajendran V, Palanichamy P. Science and technology of ultrasonic's. Alpha Science International Ltd.; UK, 2004.
9. Patange SM, Shirsath SE, Jadhav SP, Hogade VS, Kamble SR, Jadhav KM. Elastic properties of nanocrystalline aluminum substituted nickel ferrites prepared by co-precipitation method. Journal of Molecular Structure. 2013; 24;1038:40-4.
10. Kakani SL, Hemrajani C. Text book of solid state physics. Sultan Chand & Sons, New Delhi. 1997.
11. Gorter, E. W. *Philips Res. Rep.*, 1954; 9: 295.

12. Shirsath SE, Patange SM, Kadam RH, Mane ML, Jadhav KM. Structure refinement, cation site location, spectral and elastic properties of Zn2+ substituted NiFe2O4. Journal of molecular structure. Sep., 2012; 26(1024) :77-83.
13. Mazen SA, Mansour SF, Dhahri E, Zaki HM, Elmo salami TA. The infrared absorption and dielectric properties of Li–Ga ferrite. Journal of Alloys and Compounds. 20 Feb 2009; 470(1-2):294-300.